Passive Treatment of Circumneutral Mine Drainage from the St. Louis Mine Tunnel, Rico, CO: Part 1—Case Study: Characteristics of the Mine Drainage

Terry J. Moore[1] · Arthur C. Riese[2] · Anne Lewis-Russ[3] · James P. Jonas[4] · Brian S. Johnson[1]

Abstract

This publication is a case study of the seasonal variability of mine water drainage from the Saint Louis Tunnel (SLT) at the inactive Rico-Argentine mine site located in southwestern Colorado. It is an introductory paper for the two passive water treatment system technology evaluations contained in this issue. Mine water chemistry changes from baseflow to a snowmelt runoff event (SMRE) where snowmelt runoff follows preferential migration pathways to flush acidic weathering products from the upper mine workings to the SLT. Baseflow mine drainage is characterized as circumneutral, with Zn, Cd, Mn, and Ni concentrations primarily in the dissolved form. Dissolved Zn, Mn, Fe, and potentially Cd illustrate equilibrium with carbonate minerals. Total concentrations of Fe, Cu, Pb, and As are primarily in the suspended form and suggest sorption to Fe oxides. Mine water chemistry during the SMRE reflects mixing of circumneutral baseflow waters with more acidic waters flushing the upper mine workings. Geothermal activity provides for a consistently warm mine water discharge from the SLT. The two seasons that provide the most challenge to passive water treatment of SLT mine drainage are the SMRE period and the low flow stage of the Dolores River. Mine water flow and chemistry during SMRE are highly correlated with Dolores River flow and this site conceptual model was and will be used to assist in pilot project evaluation, water treatment system design, monitoring system design, a seasonal compliance approach, and water management.

Keywords SRB · Sulfide · Cadmium · Copper · Iron · Manganese · Zinc · High elevation · Colorado · Telemetry · Constructed wetlands · Biotreatment · Smithsonite · Rhodochrosite · Siderite · Snowmelt

Introduction

The St. Louis Tunnel (SLT) of the Rico-Argentine Mine Site (Rico site), Colorado, discharges on average 2600 L per minute (Lpm; 680 gallons per minute [gpm]) of circumneutral water containing elevated concentrations of Cd, Cu, Fe, Mn,

Anne Lewis-Russ is Retired, 205 Lafayette Str, Brandenburg, KY, 40108, USA.

✉ Terry J. Moore
terry.moore.texas@gmail.com

1 Atlantic Richfield Company, 201 Helios Way, Houston, TX 77079, USA

2 EnSci Inc, 1501 East Quincy Ave, Cherry Hills Village, CO 80113, USA

3 205 Lafayette Str, Brandenburg, KY 40108, USA

4 Alloy Group, 406 E. Park Ave, Anaconda, MT 59711, USA

and Zn, as well as lesser concentrations of As, Pb, and Ni. The mine water since the mid-1980s has flowed through a collapsed portal (filled with rubble and rock) followed by a series of settling ponds before the water is discharged to the Dolores River. Site-specific surface water discharge standards have not been established; however, the EPA and one of the potentially responsible parties are developing a final mine water management strategy. Because of the mountainous location, the Rico site is challenging to access, especially during the winter, and is sometimes inaccessible owing to deep snow and/or avalanche hazards. Therefore, demonstration-scale, passive treatment systems are being evaluated as management alternatives for SLT discharges. This paper provides a site conceptual model that describes the sources, migration pathways, chemical composition, and seasonal variability of discharge flow that is important for developing, operating, and evaluating passive biotreatment systems. Two of the demonstration-scale systems evaluated at the site are presented as companion papers, Parts 2 and

3, in this issue of MWE (Dean et al. 2022; Sobolewski et al. 2022).

Background

This site is in the Rico Mountains of southwestern Colorado near the town of Rico, Dolores County. The Rico Mountains are a group of 3700-m (12,000-ft) peaks at the southwest edge of the San Juan Mountains, close to the margin of the Colorado Plateau and Rocky Mountain physiographic provinces. The Rico Mountains have been uplifted, resulting in an elliptical shape, referred to as the Rico Dome. The Rico Dome is bisected by the Dolores River, which flows southward through the mountains. Downcutting and erosion by the Dolores River have produced a valley with relief of more than 910 m (3000 ft) (Pratt et al. 1969). Lower mountain slopes are mantled by a thick cover of colluvium, talus, and landslide debris. The river channel and adjacent, low-lying area is predominantly a floodplain situated at an average elevation of 2700 m (8800 ft).

The climate is characterized as semi-arid with long-duration, cold, snowy winters and short-duration, moderately wet, warm summers. The mean annual temperature near Rico is 3.7 °C (38.7 °F), averaging about 13 °C (55 °F) during the summer and −14 °C (6.5 °F) during the winter. The mean annual precipitation is ≈ 690 mm (27 in), and average annual snowfall is 4390 mm (173 in) per year.

A diagram of the Rico site is contained in Fig. 1. The town of Rico is situated on the banks of the Dolores River and the SLT portal is shown north of Rico on the site of former mineral processing facilities and settling ponds. Mine workings are at elevations > 2750 m (> 9000 ft) and are situated along the Black Hawk Fault (Fig. 1). The mining objective was epithermal deposits resulting from circulation of geothermal fluids in faults and interacting with carbonate materials. Two groups of mine workings developed over time, the Mountain Spring-Wellington Group and the Rico Argentine Group (McKnight 1974). During the 1930s, the SLT was driven at a grade of 0.4% into the mountain 1.5 km (5000 ft) and two cross cuts were constructed to provide mine drainage and transport of ore. The NW Crosscut connected to the Mountain Spring-Wellington Group and the SE Crosscut connected to the Rico Argentine Group to the SLT system. Active mining in the area ceased around 1971. Exploration occurred during the late 1970s and early 1980s during which time a significant molybdenum deposit was identified in the deeper geothermal system; but it was never developed. The portal to the SLT was open until the late 1980s, and mine water flowed through a series of ponds (with periodic lime treatment)

before discharge to the Dolores River (Paser 1996). In the late 1980s, disturbance of the site resulted in collapse of the SLT portal, and mine water continued to emerge from a permeable plug of rock and rubble. In 2001, dispersed surface flows from the collapsed SLT portal area were collected into a common channel, diverted through a Parshall flume (now designated as monitoring station DR-3), and more securely routed to a system of ponds (referred to as the St. Louis Ponds) to enhance particulate metals settling prior to release of water from the ponds to the Dolores River. In 2015–2016, two relief wells were directionally drilled to assist the drainage of the SLT tunnel to the DR-3 monitoring station.

Water that exits the SLT derives directly from seepage into the tunnel and crosscuts, as well as from the large system of interconnected mine workings that serve as conduits for the mine water that enters the mine through numerous major and minor faults, interconnected fractures, joints, and exploration drill holes. Known workings, particularly of the Mountain Spring-Wellington Mine Group and the Rico-Argentine Mine Group are illustrated in Fig. 2. Both mine groups have complex, multi-level workings in carbonate-hosted deposits that are closely associated with faulting and are connected to the SLT at a low level by two crosscuts. The SLT and crosscuts together act as a drain for natural seepage and mine water. The recharge area of the SLT and associated mine workings is estimated to comprise a watershed of ≈ 39 km^2 (15 mi^2).

A detailed presentation of the geology and composition of the epithermal deposits comprising the materials mined from the Mountain Spring-Wellington and Rico Argentine Groups is contained in the work of Hudson et al. (1997), Larson (1987) and McKnight (1974). The sulfide minerals of mining significance included pyrite, sphalerite, galena, and chalcopyrite. Common gangue/secondary minerals included quartz, fluorite, calcite, dolomite, manganoan siderite, rhodochrosite, rhodonite, smithsonite, and sericite. Weathering of sulfide systems which contain significant carbonate minerals can create circumneutral mine drainage (Desbarats and Dirom 2006; Lindsay et al. 2015; Nordstrom 2011a; Plumlee et al. 1999). The inactive Myra Mine (British Columbia) produced Cu and Zn from a massive sulfide deposit with carbonates and produces year-round flow of circumneutral mine water discharge from an underground tunnel (Desbarats and Dirom 2006). At that site, seasonal changes in mine water chemistry are associated with flushing of the mine by heavy rainfall events in the fall, analogous to the spring freshet events during snowmelt at the Rico site.

The hydrothermal system beneath the Rico site has a high geothermal gradient (> 80 °C/km) that suggests economically viable geothermal energy resources (Sares et al. 2009). Hot springs and vent wells are present at the site and produce
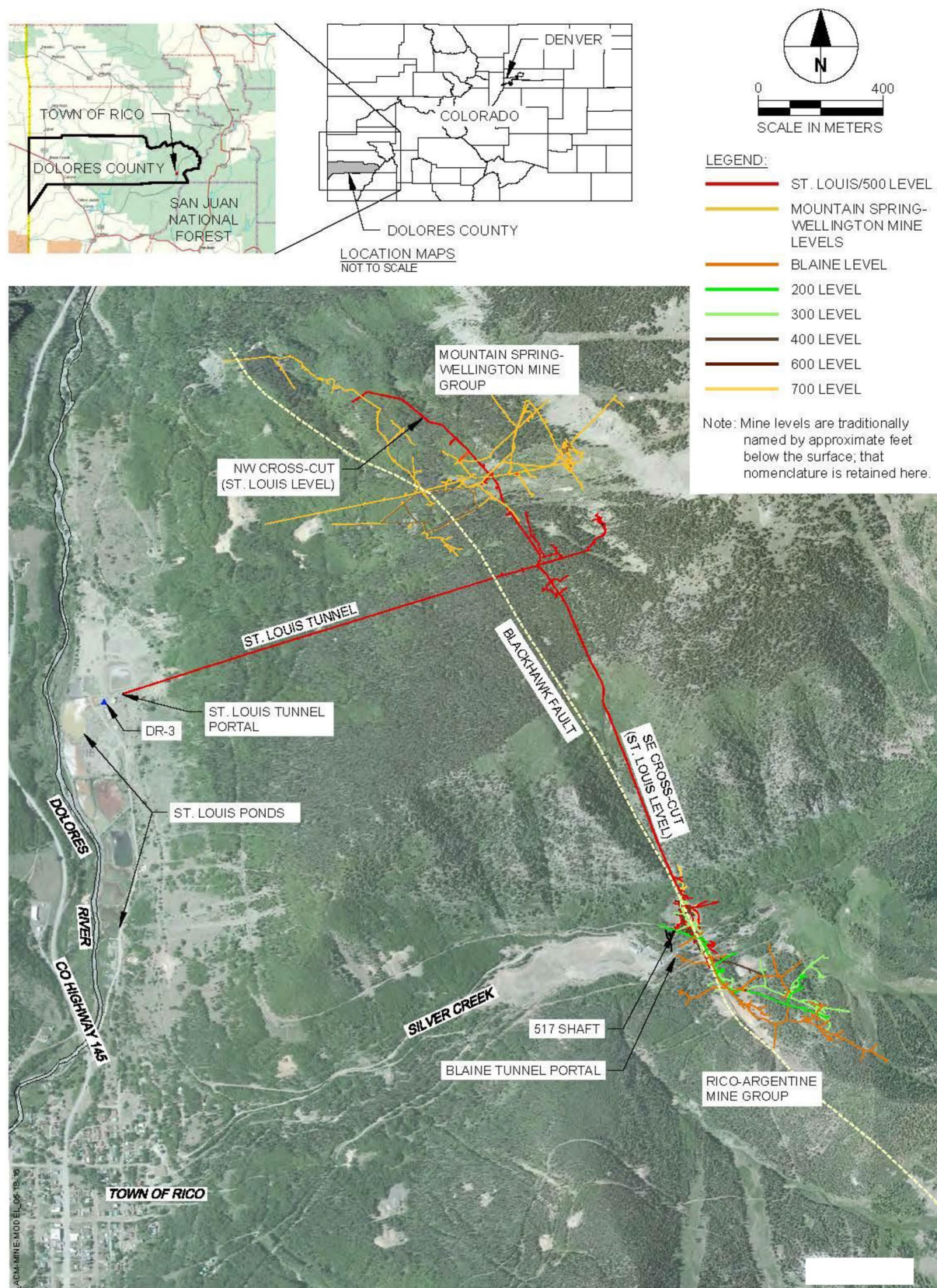
Fig. 1 Diagram of mine workings reporting to the Saint Louis Tunnel over a 2012 aerial photograph
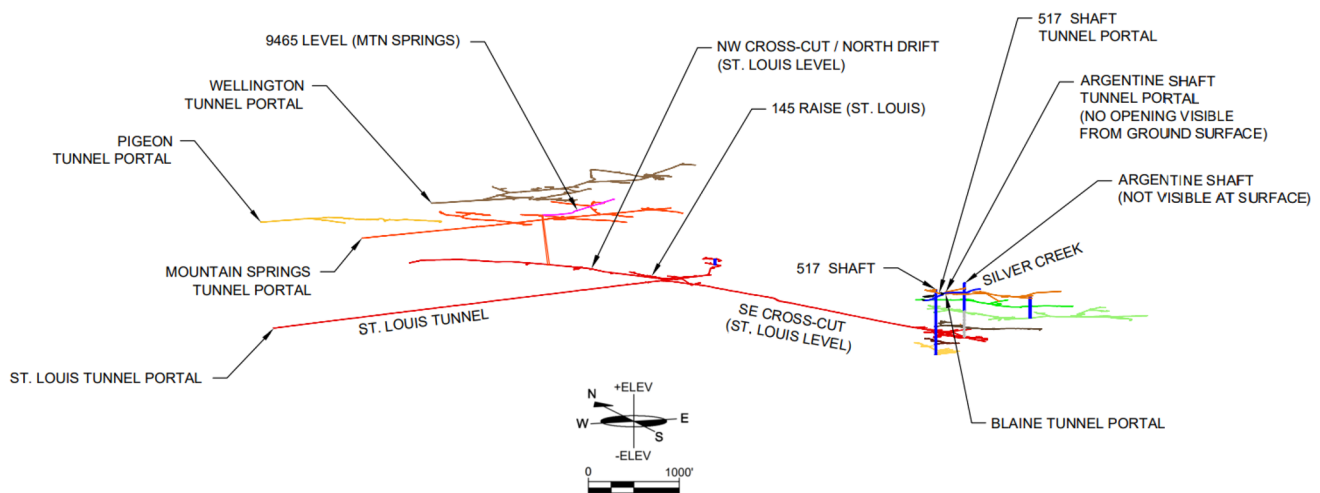
Fig. 2 Oblique diagram of the mine workings and crosscuts that report to the Saint Louis Tunnel

year-round flow of warm water to the surface. Flow of warm water from the SLT will benefit passive treatment systems in the harsh winters at the site.

Work has occurred and is ongoing at the St. Louis Ponds portion of the Rico-Argentine Mine Site Rico - Tunnels Operable Unit 01, under a 2011 Unilateral Administrative Order (US Environmental Protection Agency [USEPA] 2011a), a Removal Action Work Plan (RAWP) (USEPA 2011b), a 2021 Administrative Settlement Agreement and Order on Consent for Removal Action (USEPA 2021a), and an updated Removal Action Work Plan (USEPA 2021b). As a key task under the RAWPs, tests of wetland technologies began in 2012 and are ongoing, including a pilot-scale wetland and larger wetlands systems, with both horizontal-flow and vertical-flow anaerobic sulfate-reducing process steps. The two passive system studies were conducted in 2015 and 2016 and are the subject of two companion articles in this issue. A larger, demonstration-scale semi-passive treatment system was completed in 2017, with more than 1900 Lpm (500 gpm) capacity, and presently treats the majority of baseflow from the SLT. Evaluation of this demonstration-scale system is the subject of a publication in progress. The SLT discharge data collected from 2014 to 2020 are the subject of this publication, which presents the site conceptual model for evaluation of technology and management of the SLT discharge.
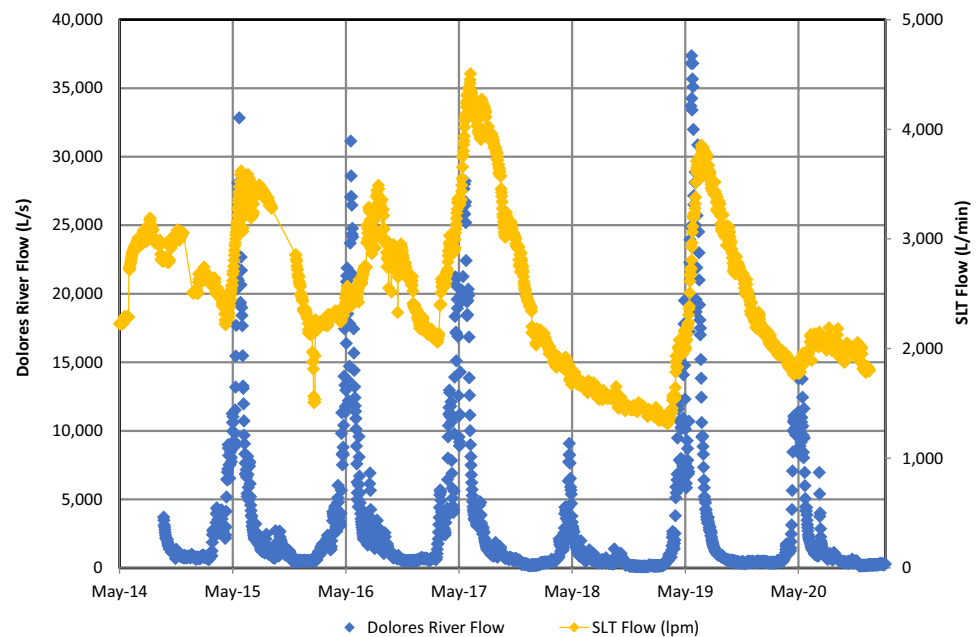
Methods

Mine water characterization data for this study were collected at the DR-3 sampling station for both flow and water chemistry (Fig. 1). The mine water that emanated from the SLT through the rock and rubble of the collapsed portal and

surface flowed to the DR-3 sampling location where discharge flow measurements were conducted using a modified Parshall flume. Relief wells were installed behind the collapsed portal in September 2016, and mine water currently flows through these wells to the DR-3 location, although lessor volumes still discharge from the debris plug. Pressure transducers at DR-3 downloaded measurements at 15-min intervals and require monthly cleaning. A YSI EX02 sonde (measuring pH, oxidation/reduction potential (ORP), dissolved oxygen (DO), temperature, specific conductance, and turbidity) was used to collect water quality parameters at 15-min intervals. Values of ORP are uncorrected and are expressed as mV relative to an Ag/AgCl reference electrode (3 M KCl). The sonde was equipped with wipers to limit fouling of the sensors and was calibrated monthly or as needed. Data were collected using data loggers and later using an HDMI and telemetry system that are also accessible via the internet to off-site project personnel. The telemetry system also transmitted data from a site camera and an on-site weather station.

Sampling of mine water discharge at DR-3 was conducted using standard EPA methods (USEPA 1993, 1994) and Level IIB QAQC protocols (USEPA 2017). Sampling events were performed approximately monthly from 2014 to the end of 2017, with more frequent sampling as needed during freshet events. Sampling frequency was reduced to bimonthly beginning in 2018. Field parameters were collected using portable equipment for pH, temperature, conductivity, turbidity, ORP, and DO. Instruments were calibrated at least daily and monitored using standards for drift during the day. The values of field parameters are presented in this paper (more accurate) and sonde data are used to study shorter-scale time variability (more frequent data). Metals and As were analyzed using EPA Method 200.8

Fig. 3 Relationship between St. Louis Tunnel flow with Dolores River flow rate. St. Louis Tunnel discharge measured near portal (DR-3); Dolores River flow rate measured at USGS gage 09165000 located about 7 km downstream of the site

(USEPA 1994) and samples were collected for both total and dissolved (0.45 mm filtered) metals. Collection and analysis protocols for sulfides (SM 4500S2D), TSS (SM 2540D) and alkalinity (SM 2320B) are from APHA (2005), and sulfate (EPA 300.0) is from USEPA (1993).

Dolores River flow data were obtained from the USGS on-line database. Data for the "Dolores River below Rico" (USGS Sta. 09165000) were used to represent the Rico site, although minor additional flows from Silver Creek occur between the site and the USGS monitoring station (USGS 2022). Snowpack estimates were from the SNOTEL database and the Scotch Creek site was used as most representative of site conditions (USDA NRCS 2021).
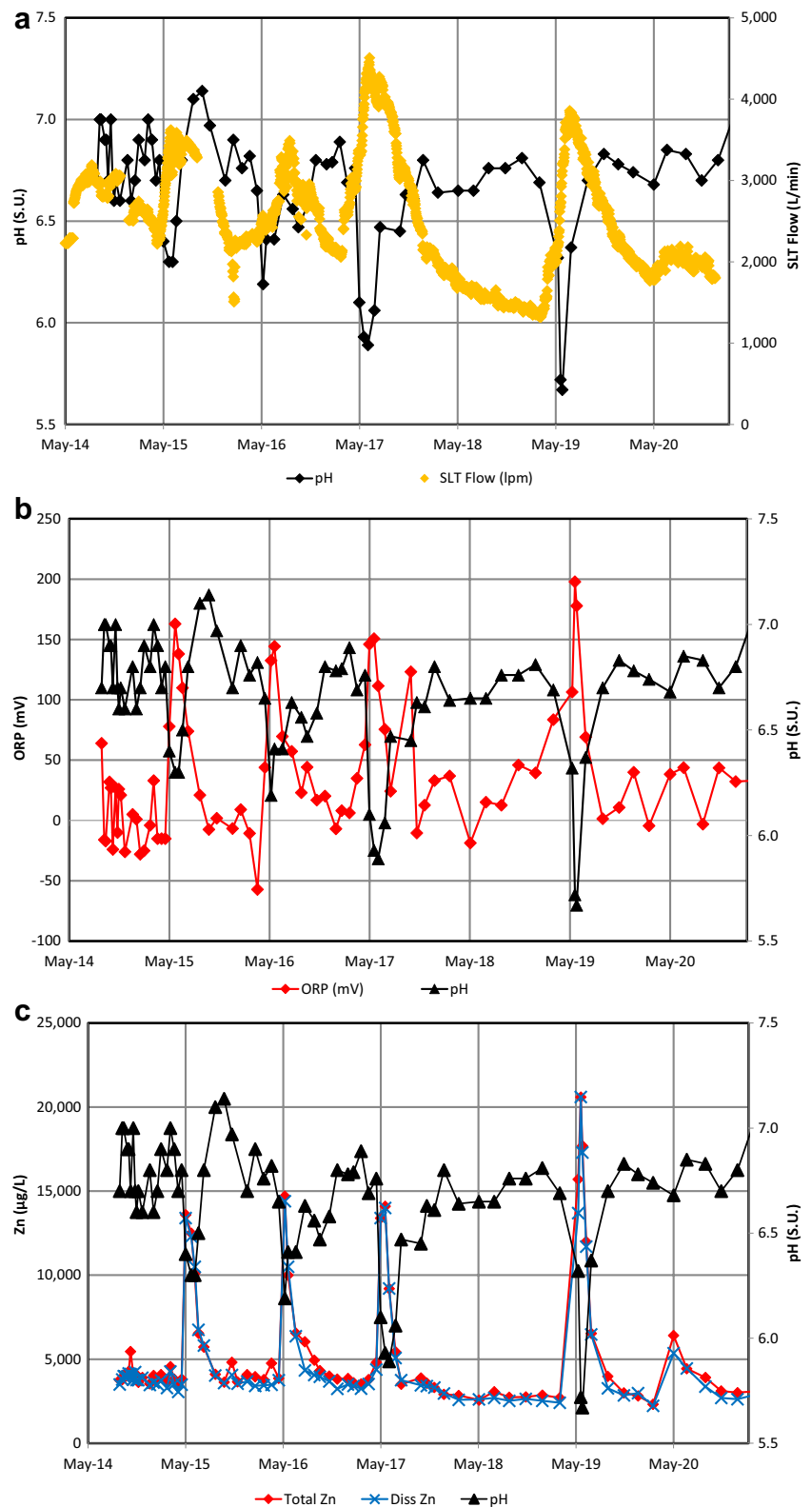
Results

Hydrographs for the mine water discharge from the SLT (monitoring point DR-3) and Dolores River flow are shown for 2014–2020 in Fig. 3. The SLT hydrographs for each year show minimum SLT flow at the end of winter when the ground and surfaces are frozen. As temperatures rise in March, snow begins to melt, infiltrate, recharge groundwater, and increase the SLT flow rate. Ice in the mine workings begins to melt as well. The SLT hydrograph increases with the increasing rate of snowmelt and surface water runoff and reaches a maximum in mid-June. Following snowmelt, the hydrograph declines as surface water contributions slow, infiltration is reduced and groundwater from storage becomes the dominant contribution to the hydrograph and flows from the SLT. Summer monsoon rains can slow the decline of the hydrograph as it declines to a minimum in

winter months. The 2016 water year contained heavy rains in the later summer and fall that caused a late peak in the hydrograph around the first of September. Mine water flow from the SLT is driven predominantly by snowmelt infiltration and groundwater recharge, with flow rates ranging from 1342 to 4453 Lpm (353–1172 gpm) and a maximum value 3.3 times that of the minimum (2014–2020). The rising limb of the hydrograph for the Dolores River is driven predominantly by snowmelt runoff and demonstrates a more abrupt rise and fall of the hydrograph with the peak corresponding to maximum snowmelt runoff rates. The Dolores River flow ranges from 116 to 36,812 Lps (30 to 9687 gps) reaching a maximum value of 317 times that of the low-flow rate in late fall and winter. Peaks of the SLT hydrographs occur from mid-June to mid-July, except for 2016 (dominated by late summer rains) and 2018 and 2020 when minimal snowpacks occurred. Peak Dolores River flows occurred with a narrow range of May 31 to June 11 during the study period, from 2014 to 2020.

Seasonal variability of SLT mine water flow and chemistry present a challenge to evaluating, designing, and operating passive biotreatment systems at the Rico site. A time-series plot of pH and SLT flow is contained in Fig. 4a. Consistent values above pH 6.6 occur throughout most of each year, with annual low-pH events occurring in late-May to early-July. The pH drops from circumneutral to slightly acidic during this time each year, with a minimum value of 5.67 in 2019. Depressions in pH occur most years during the SLT flow rise, prior to the peak of the hydrograph. One pH-low also occurred during the later-summer of 2016, when high rainfall and runoff created a second later peak in SLT flow rates. Values of ORP also change during
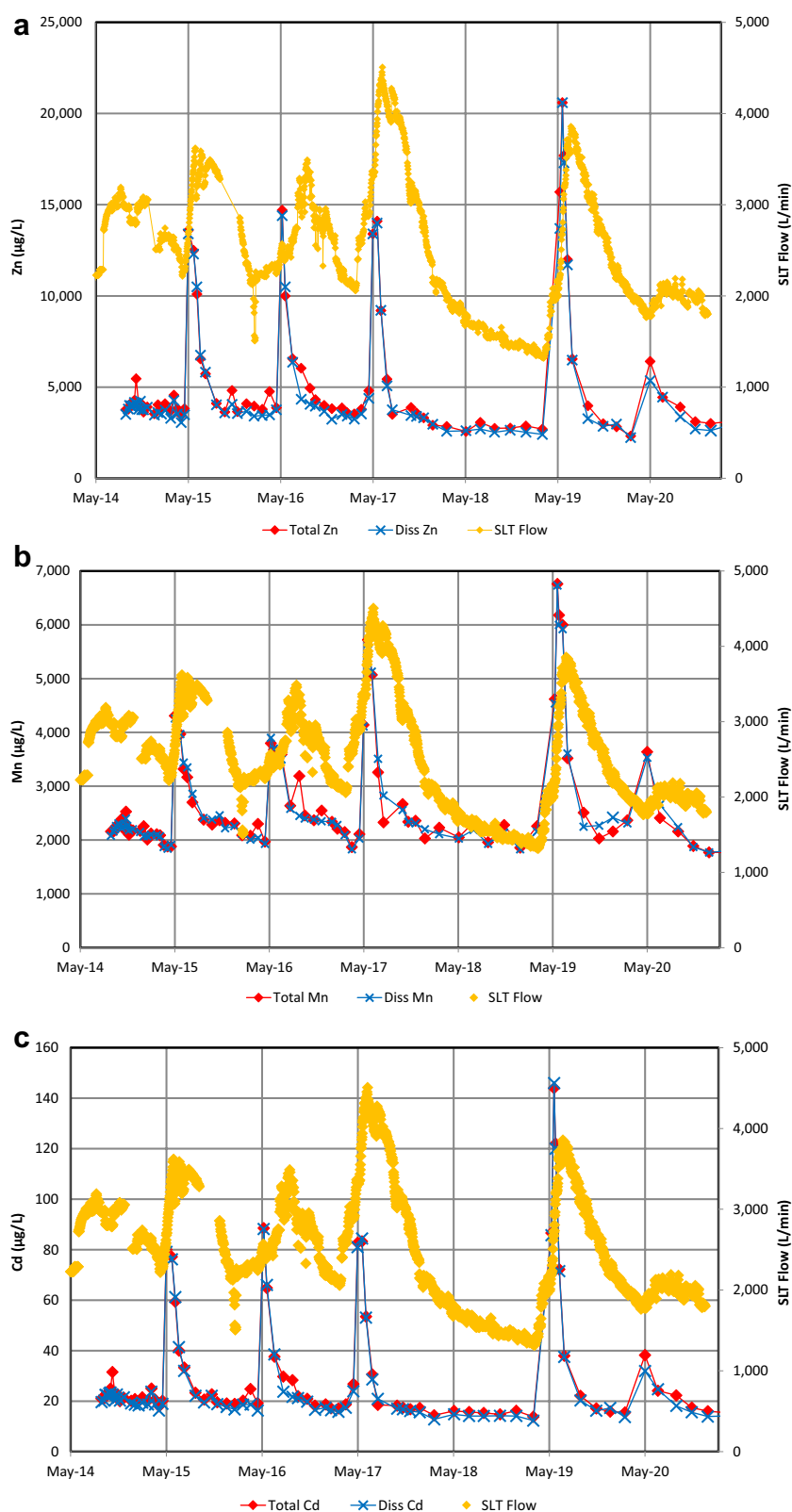
Fig. 4 **a–c** Time-series plots of pH with SLT flow, ORP, and Zn concentrations of mine discharge water from the SLT at monitoring location DR-3 over the course of the study. Peak flow of the SLT snowmelt freshets occur in mid-May, approximately at vertical hashmarks

the low-pH event, but peak values are antithetic and rose from a baseflow of −28 to 20 mV to a maximum value of 197 mV during 2019 (Fig. 4b). The low-pH event each year

is accompanied by high metal concentrations, shown here with an example of Zn concentrations (Fig. 4c). Metals with a similar high-metal response during the low-pH event each
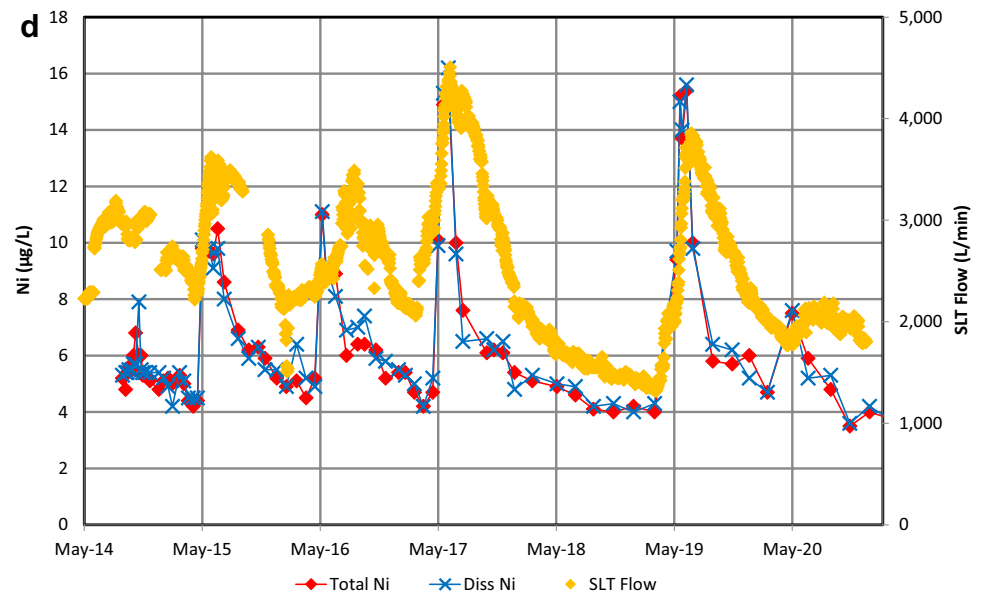
Fig. 5 **a–d** Relationship between St. Louis Tunnel total and dissolved metals concentrations (µg/L) and SLT flow rates (L/s). This figure included metals dominated by the dissolved fraction: **a** Zn, **b** Mn, **c** Cd, and **d** Ni. Peak flow of the SLT snowmelt freshet occur near vertical hashmarks in mid-May

year are represented as time-series plots of total and dissolved metals concentrations with the SLT hydrograph in Fig. 5a–d for Zn, Mn, Cd, and Ni, respectively. These metals

occur at relatively consistent concentrations until the low pH event, which occurs during the rising limb of the SLT hydrograph (mid-May to mid-June). The time-series plots of

Fig. 5 (continued)

other metals that do not show consistent increases of concentrations solely during the low-pH events are contained (along with the SLT hydrograph) in Fig. 6a–d for Fe, Cu, Pb, and As, respectively. Copper shows intermediate behavior, with peaks in dissolved Cu during low-pH events in 2015, 2016, 2017, and 2019 (Fig. 6b).

Average baseflow mine water composition is summarized in Table 1, along with water chemistry for the lowest pH-event that occurred during the 2019 season. The mine water is a Ca-sulfate type water for both baseflow and low-pH events, as is consistent with most circumneutral mine waters. Calcium and sulfate concentrations suggest the waters are about 30–50% saturated with gypsum during baseflow. The total metals data illustrate an increasing magnitude of metals concentrations in average baseflow such that As, Ni < Pb, Cd < Cu < < Al < Mn, Zn < Fe, whereas dissolved metals show Al < Mn, Fe < Zn. Filtration of samples using a 0.45 μm membrane is used for monitoring purposes and terminology of dissolved metals is used here for filtered samples, although some particulates may pass through the filter membrane. Dissolved metals analysis for Zn, Mn, Cd, and Ni show that dissolved concentrations are > 90% of total metals concentrations. Sulfate comprises 87% of the anion mass (mg/L) and 78% of the charge balance (mEq/L; Table 1). The pH of the average baseflow is 6.77, with a low pH of 5.76 during 2019 (the most intense low-pH event of the study). ORP values are inverse of pH with an average ORP of 15 mV during baseflow and an ORP of 198 mV during the 2019 low-pH event. Carbon dioxide occurs in high concentrations in the SLT mine water and partial pressure of CO_2 (P_{CO2}) was calculated for selected water samples during baseflow and the 2019 low-pH event. The speciation code PHREEQ was used to speciate and determine P_{CO2} from pH,

alkalinity, ionic strength, and temperature. Values of P_{CO2} were 0.031 and 0.064 atm for the baseflow mine drainage and low pH conditions, respectively (Table 1).

Correlations of dissolved metals, pH, ORP, and total suspended solids (TSS) are contained in supplemental Table S-1 and suspended metals and TSS correlations are contained in supplemental Table S-2. The metals Zn, Mn, Cd, and Ni are contained primarily in the dissolved fraction and have a strong negative correlation with pH and a positive correlation with ORP (Table S-1). Metals contained primarily in the suspended fraction (Table 1) show a strong positive correlation between Fe, Al, Cu, Pb, As, and TSS (Table S-2). The suspended concentrations of Al and Cu correlate with other suspended metals during baseflow conditions, but dissolved concentrations increase significantly during low-pH events. The metal Cu has the greatest peak concentration divided by average baseflow concentrations of any metal, with a ratio of 100 (Table 1).

Passive biosystems are often not evaluated in high-altitude alpine locations due to the important effect of water temperatures on biochemical reactions. Geothermal energy contributes to the stable monthly average temperatures of discharge from the SLT compared to the monthly ambient air temperatures shown in Fig. 7. Average monthly temperatures of SLT discharge range from 17.8 to 20.5 °C (64.0–68.9 °F), whereas average monthly temperatures for ambient air on the site range from − 14.9 to 19.2 °C (5.18–66.6 °F). Lower SLT discharge temperatures correspond with highest flows from the SLT and represent the largest flow of snowmelt-derived groundwater through the geothermal system. The consistently warm mine water

Fig. 6 a–d Relationships between St. Louis Tunnel total and dissolved metals concentrations (µg/L) and SLT flow rates (L/s). This figure includes metals dominated by the suspended fraction: **a** Fe, **b** Cu, **c** Pb, and **d** As. Peak flow of the SLT snowmelt freshet occur near vertical mid-May hashmarks
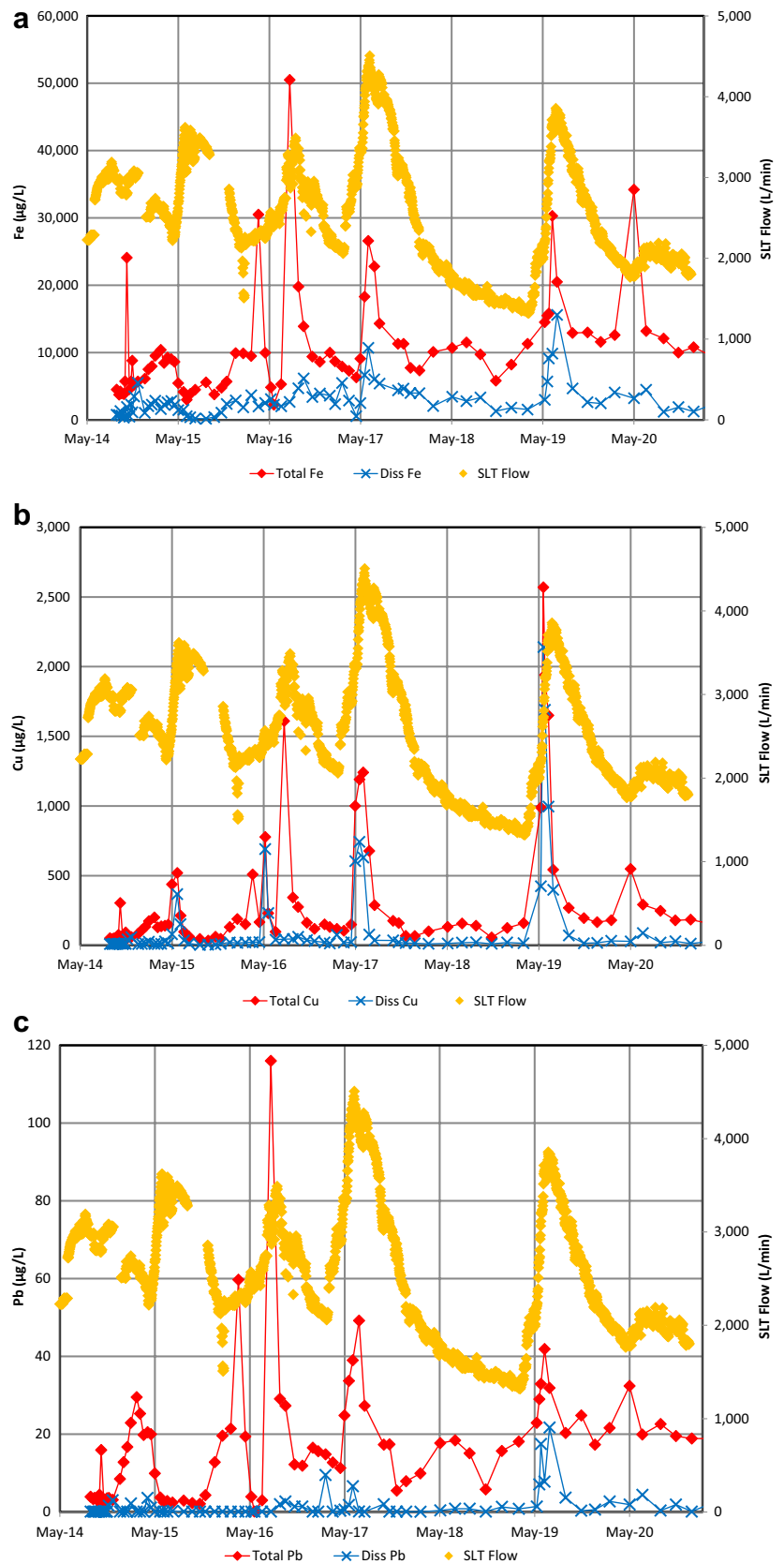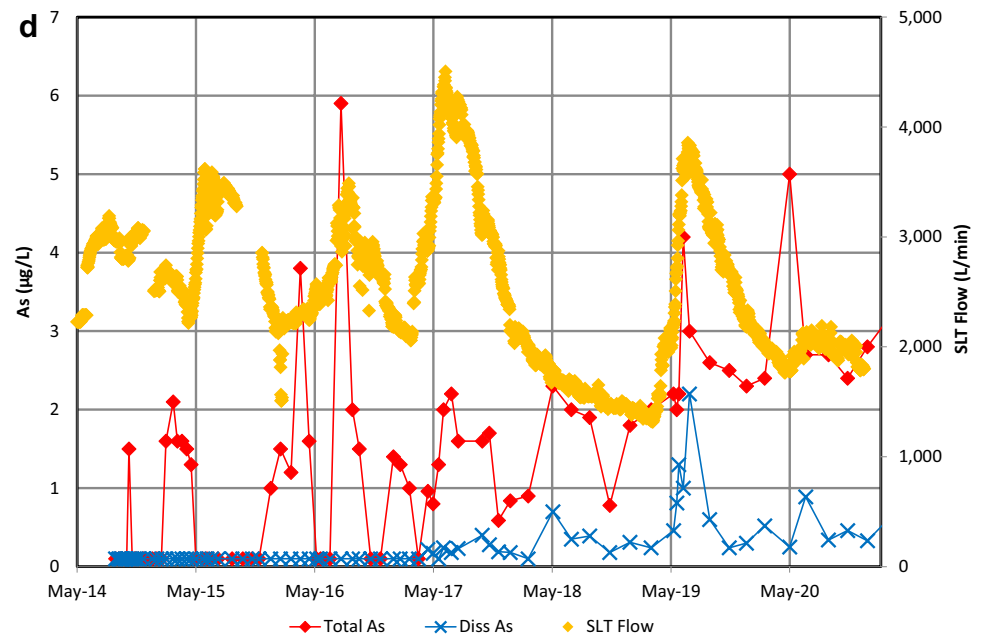
Fig. 6 (continued)

discharge is somewhat unique to the SLT system and adds to the efficiency of passive treatment systems at the site.

Discussion

Hydrology of the SLT Discharge

The annual hydrographs for flow from the SLT consist of a baseflow component related to capture of groundwater and a flashy snowmelt runoff component that results from snowmelt runoff entering the mine workings via preferential pathways. Hydrographs for SLT baseflow are derived from infiltration and recharge, followed by capture of groundwater in the lower mine workings and natural faults (many mineralized) that interconnect with the SLT workings. Snowmelt provides the greatest source of water for groundwater recharge and the hydrograph peaks roughly correlate with peak annual snowpack (supplemental Fig. S-1). Correspondingly, very limited hydrograph peaks occurred during 2016 (minor), 2018 (none), and 2020 (minor), and are associated with the years when the snowpack is low (Fig. 3). Summer rain events dominate the freshet peaks in 2016 and 2020 and these hydrograph peaks, of smaller magnitude, are shifted to later summer. The 2018 season lacked sufficient snowpack or rainfall, so no hydrograph peak resulted, with SLT flow continuing to decrease to the end of 2018. The Dolores River hydrograph is dominated by snowmelt runoff and is also displayed in Fig. 3 to illustrate how SLT snowmelt runoff could contribute to the SLT hydrograph. Studies of the Dolores and Colorado River hydrographs indicate that the rising limb of the river hydrograph is driven by snowmelt

runoff, with the timing and rate of release affected primarily by dust radiative forcing in snow (Bryant et al. 2013; Painter et al. 2007, 2018). Snowmelt runoff contribution to the SLT flow occurs as a small peak in the same relative position as the Dolores River hydrograph peak during 2016 and 2020 (Fig. 3). Contributions of snowmelt runoff to the SLT hydrograph for the years 2015, 2017, and 2019 correspond with the Dolores River hydrographs and consist of a steepening of the hydrograph during the rising limb of the SLT hydrograph. The contribution of snowmelt runoff to the SLT hydrograph is important because of changes to the chemistry of SLT flow. Figure 8 relates total Zn concentrations in SLT mine water discharge to the hydrograph of the Dolores River (analogue for SLT snowmelt contribution) and the correlation is striking in the timing, duration, and intensity of the annual events. This suggests that the same mechanism that drives the rising limb of Dolores River flow (snowmelt runoff) also drives Zn concentrations in SLT discharge.

The SLT drainage basin is 39 km^2 (15 mi^2) and surface drainage features tend to follow the surface expressions of faults. Infiltration of snowmelt and rainfall in the basin is the primary contributor to groundwater recharge and SLT flow. Drainage patterns funnel snowmelt runoff water to the surface expressions of faults in the SLT watershed, the most pronounced being the Blackhawk fault. This fault is known to have preferential flow pathways that rapidly transmit surface water to the mine workings (Cowie et al. 2014; McKnight 1974; USEPA 2012, and other unpublished mining reports). Contributions may also occur year-round where the Blackhawk fault crosses the saturated alluvium of Silver Creek (Cowie et al. 2014; McKnight 1974; USEPA 2012). The mining record contains references to the hanging wall

Table 1 Mine water analytical data collected at DR-3 for average base flow and the 2019 peak SMRE (most intense event)

Analyte	Average base flow			2019 peak SMRE			Dissolved/total (%)		2019 peak SMRE/base flow (Dissolved)	Diss Me/Fe
	Total	Diss	Susp	Total	Diss	Susp	Average Base Flow	2019 Peak SMRE		Average base flow
pH (S.U.)		6.77			5.67					
ORP (mV)		15			198					
Fe (µg/L)	10,005	2460	7545	50,500	15,600	34,900	24.6	30.9	6.3	
Al (µg/L)	1006	108	898	7040	5440	1600	10.8	77.3	50.3	0.044
Zn (µg/L)	3763	3453	310	20,600	20,600	0	91.8	100	6.0	1.40
Mn (µg/L)	2206	2176	29.7	6760	6730	30	98.7	99.6	3.1	0.885
Cu (µg/L)	168	21.3	146	2570	2140	430	12.7	83.3	100	0.009
Pb (µg/L)	16.3	<0.8	15.5	116	21.7	94.3	5.0	18.7	NC	NC
Cd (µg/L)	20.0	18.4	1.6	144	146	0	91.9	101	7.9	0.007
Ni (µg/L)	5.3	5.2	0.1	16.2	15.5	0.7	97.7	95.7	3.0	0.002
As (µg/L)	1.3	<0.2	1.1	5.9	2.2	3.7	14.8	37.3	NC	NC
Ca (mg/L)	242	240								
Mg (mg/L)	192.0	18.7								
Na (mg/L)	10.0	9.6								
K (mg/L)	1.7	1.7								
Alkalinity (mg/L)		104			21.4					
Sulfate (mg/L)		635			908					
Sulfide (mg/L)		<0.05								
PCO2 (atm)		0.031			0.064					

Data are provided for total, dissolved (Diss), and suspended (Susp) forms

NC—Not calculated because of <DL data

Me—Refers to concentration of each metal analyte in Table 1 divided by Fe concentration

Limited analyses for major cation and anion data (2 samples)

Sulfide data for (DR-3) were collected during 2014 and discontinued afterward, as the median value was <0.05 mg/L (RL)

Analyses include total, Diss (dissolved, <0.45 µm filtered), and Susp (suspended, total-dissolved)

Fig. 7 Time-series plot of SLT mine water temperature (Celsius) measured at DR-3 with ambient air temperatures measured on site
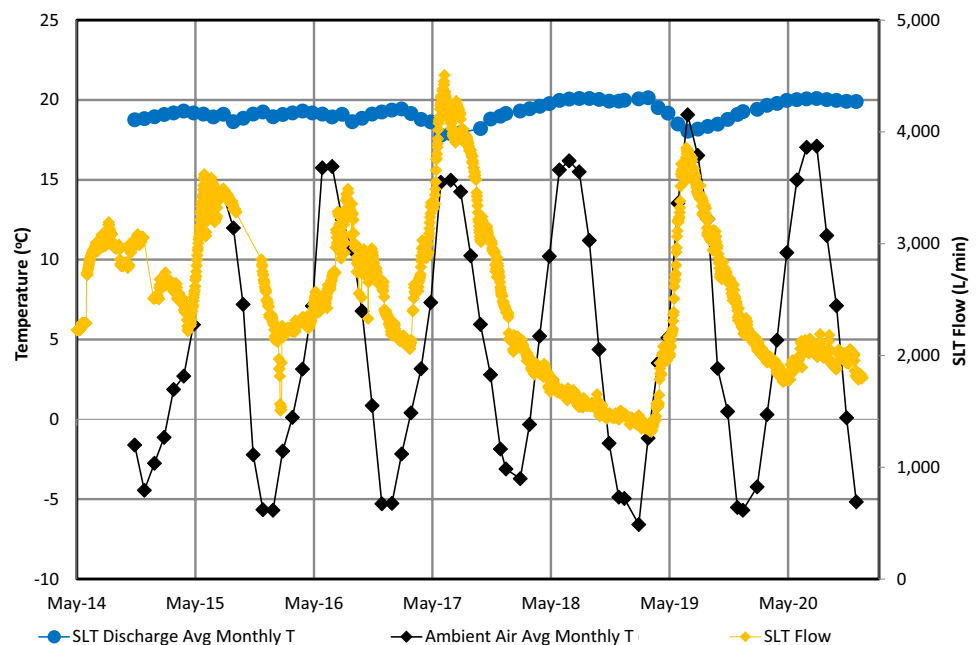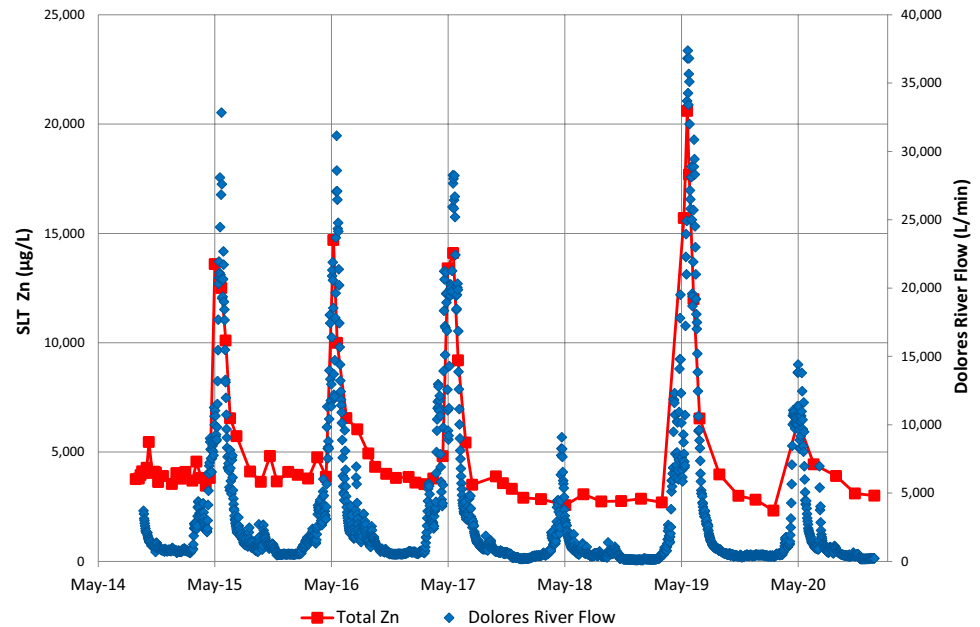
Fig. 8 Time series plot of total Zn in SLT mine water with Dolores River flow.

of the fault producing significant amounts of water to mine workings during the snowmelt season and in proximity of Silver Creek. Earlier work at the site used tracers to characterize the flow path between the Blaine Tunnel and the SLT discharge (Cowie et al. 2014; USEPA 2012). The study showed a direct connection with an 18-h travel time and limited dispersion. The SLT hydrograph has two components: (1) baseflow originating from groundwater recharge and capture that produces a rise of flow in the spring through fall, and (2) flow that also includes contribution of snowmelt surface runoff to SLT flow, which appears as a short duration steepening of the rising limb of the SLT hydrograph and is analogous to the Dolores River hydrograph shown in Fig. 3. The groundwater captured in the SLT is henceforth referred to as baseflow and the period where significant snowmelt surface water runoff is also captured by the upper workings of the SLT is referred to as the SLT snowmelt runoff event (SMRE).

The SE Crosscut (Fig. 2) water flow and chemistry have more recent data because of modifications and maintenance of the mine systems draining to it and studies that have been recently completed. The mine workings draining to the NW Crosscut and SLT have only mine water chemistry and flow data from Aug. 18, 1980 (Whyte 1982) when personnel could access the SLT at the point where the NW and SE crosscuts and 145 Raise join the SLT (Fig. 2). Data for flow estimates and metals concentrations are included in Table 2. Estimated flow from the SE and NW crosscuts and 145 Raise were estimated as 67%, 25%, and 8%, respectively (based on observation of total flow). Estimated metals load values for the NW crosscut (Table 2) indicate the percentage of metals load originating from the NW Crosscut for Cd, Fe,

and Zn were 82%, 90%, and 79%, respectively. Although pH values for drainage were compromised, higher metals concentrations in the NW crosscut suggest that the mine water pH values may have been lower.

Chemistry of Baseflow Mine Water

Baseflow conditions of SLT discharge (outside the SMRE of mid-May to mid-July) resulted in relatively consistent water chemistry over time as shown in the time-series plots of Figs. 5a–d and 6a–d. Slightly lower baseflow metals concentrations occurred during the summers of 2017 and 2019 when summer rains extended the hydrographs of DR-3 flow, and during 2018 when annual snowfall, rainfall, and SLT discharge were at their lowest levels (Fig. 5a). Consistency of composition suggests that groundwater contributions from mineralized zones are responsible for the bulk of water collected by the SLT system during baseflow. Figure 9 illustrates that the SE Crosscut connects with the Rico Argentine Workings just below the 400-ft level and that much of the baseflow component of the mine drainage may be basin groundwater transported through the lower, flooded mine workings and other naturally mineralized faults and pathways. Oxygenated groundwaters in the basin enter the system through infiltration and are transported through soils, mineralized zones, and lower flooded mine workings where limited oxidation of sulfide minerals produces acidity that is neutralized by the carbonate minerals described as gangue carbonate materials including calcite, dolomite, manganoan siderite, rhodochrosite, and smithsonite (McKnight 1974). In flooded mine workings that are not fully aerated, acid generating reactions are limited and development of circumneutral

Table 2 Flow Contributions to St. Louis Tunnel 2 Flow Contributions to St. Louis Tunnel

Analyte	Units	Southeast crosscut	Northwest crosscut	145 raise	SLT portal	SLT discharge
Estimated percent flow		67%	25%	8%	Total	–
Total cadmium	mg/l	0.009	0.107	<0.001	0.022	0.029
percent total load		18%	82%	–	–	–
Total Iron	mg/L	3.7	102	5.6	16.2	12.8
percent total load		8.6%	90%	1.6%	–	–
Total Zinc	mg/L	2.62	27	0.50	5.2	5.0
percent total load		21%	79%	0.5%	–	–
Fluoride	mg/L	2.7	18	1.7	4.3	5.8
percent total load		28%	70%	2%	–	–
Sulfate	mg/L	544	1,070	505	562	620
Percent total load		54%	40%	6%	–	–

Samples and observations collected Aug 18, 1980 (Whyte 1982)

Estimated percent flow to St. Louis Tunnel (SLT) as reported in unpublished mine report (Whyte 1982)

Percent total load accounts for percent of flow and concentration

Data from unpublished laboratory report

Sample location identified in unpublished mine report except for "SLT Discharge," which was identified on the laboratory report

Exact sample locations for "SLT Portal" and "SLT discharge" are not known but are assumed to be in close proximity near the mouth of SLT

pH of 7.0 reported for STL discharge location; others were tested from samples suspected of being acidified prior to pH analysis; for example, pH for STL Portal was 1.8

conditions can develop after flooding occurs (Demchak et al. 2004; Donovan et al. 2000; Lambert and Dzombak 2000). Dissolution of carbonate minerals can also accelerate this process producing CO_2, which is dissolved in the migrating mine water (Cravotta 2007; Kirby et al. 2009; Nairn 2013). The historic mining records at Rico also contain references to high levels of CO_2 that posed historic mining hazards (McKnight 1974). Limited air exchange in the crosscuts and SLT results from flooded conditions where the mine workings decant to the crosscuts and at the flooded SLT portal, which backs up water into the SLT (Fig. 1). Restricted aeration and presence of old mine timbers and lagging in the SLT may result in conservation of high levels of CO_2 and minimization of ferrous iron oxidation in the SLT system.

Mine water composition at the SLT portal was interpreted using The Geochemist's Workbench (Bethke and Farrell 2022). Figures 10a–c contain phase stability diagrams for smithsonite, rhodochrosite, and siderite. Chemical data from SLT discharge (differentiated as to baseflow and SMRE) and from limited data collected in the upper mine workings (Table 3) are also plotted. Mineral stability fields were calculated for P_{CO2} values of 0.031 atm (average of baseflow data), 0.064 atm (SMRE peak during 2019), and 0.01 atm. Metals concentrations of Zn, Mn, and Fe (dissolved) appear to be solubility-controlled in baseflow SLT mine water at the DR-3 sampling location. Circumneutral mine waters in other underground systems that have air exchange often contain less CO_2 and ferrous iron, pH > 7.4, are elevated in Eh and

dissolved oxygen, undersaturated with respect to carbonate phases, and with metal concentrations controlled by Fe oxide sorption (Desbarats and Dirom 2006). Baseflow SLT mine water (and even some SMRE water) is in equilibrium with respect to smithsonite (Fig. 10a). Smithsonite is typically found as a reaction byproduct of sphalerite oxidation, occurring generally beneath a water table (Ridgley 2018), as occurs at the Rico site. The dissolved Zn concentrations appear to flatten at pH values > 6.8 and could be related to dilution, or another unidentified mineral phase or ion pair. The shortfall of this type of plot is that P_{CO2} and pH values systematically change at the same time and P_{CO2} decreases as pH increases (as shown by different equilibrium lines calculated for different P_{CO2} values) and could account for the flattening of the Zn concentrations. Changing the mine water conveyance to DR-3 during the relief-well construction project allowed more water sample aeration early in the study and those higher pH baseflow values were from that period. The average of log saturation indices for smithsonite in all baseflow samples was -0.022. Calculations were made to determine if Cd concentrations were solubility controlled, but waters were consistently undersaturated with respect to otavite and other Cd minerals. The positive correlation between Zn and Cd concentrations (Table S-1) in SLT mine waters may be the result of Zn/Cd ratios in oxidizing sphalerite (or turkey fat) ores (Bao et al 2021), or the existence of a solid solution of smithsonite/otavite (Ridgley 2018). The rhodochrosite phase diagram (Fig. 10b)
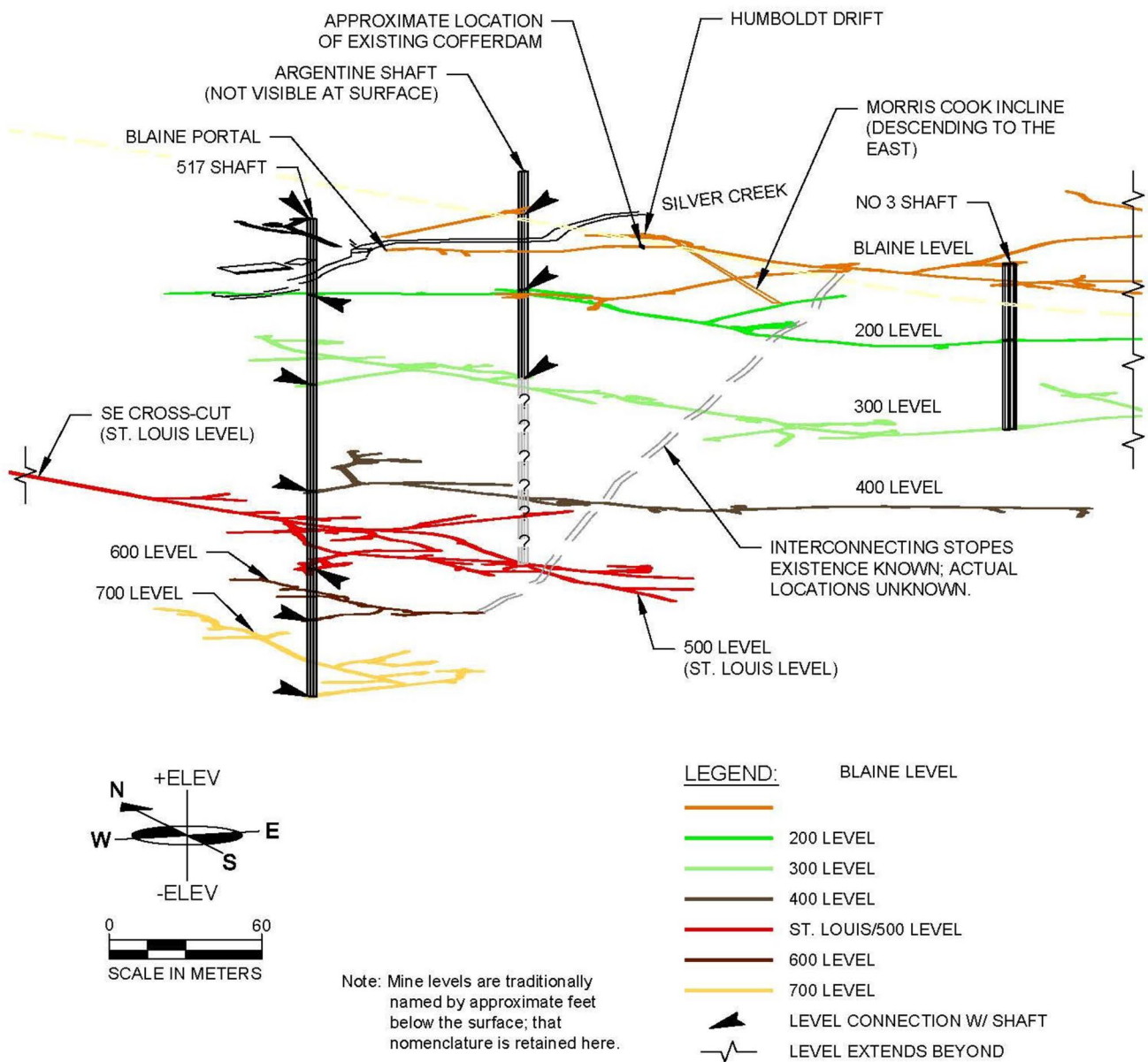
Fig. 9 Diagram of Rico Argentine mine workings reporting to the Saint Louis Tunnel

shows the baseflow concentrations of Mn are near saturation or slightly undersaturated with respect to rhodochrosite (log SI = − 0.50). The siderite phase diagram (Fig. 10c) illustrates that baseflow dissolved iron concentrations are near equilibrium or slightly undersaturated with respect to siderite (log SI = − 0.55). Saturation of SLT baseflow with respect to Zn, Mn, and Fe carbonate minerals occurs due to attenuation of acid mine drainage transported through flooded portions of the mine underground and equilibrium with the metal carbonates that occur naturally in mineralized fractures and in saturated underground mine workings. Slight undersaturation with respect to Mn and Fe carbonate minerals likely occurs because all of the SLT tunnel drainage

water does not migrate through mineralized faults and fractures during baseflow.

Thermodynamic modeling of the SLT waters (DR-3 discharge) indicates that Cu, Pb, and As were undersaturated with respect to any carbonate minerals within The Geochemist's Workbench databases and that concentrations were likely controlled by mixing circumneutral baseflow waters with other acid drainage from upper mine workings and/or sorption of metals to iron oxides. The percentage of dissolved concentrations (M(diss)/M(total)) in baseflow for these metals are low, with averages of 13%, 5%, and 15% for Cu, Pb, and As, respectively (Table 1). The As ratio is artificially high as both total and dissolved As concentrations are
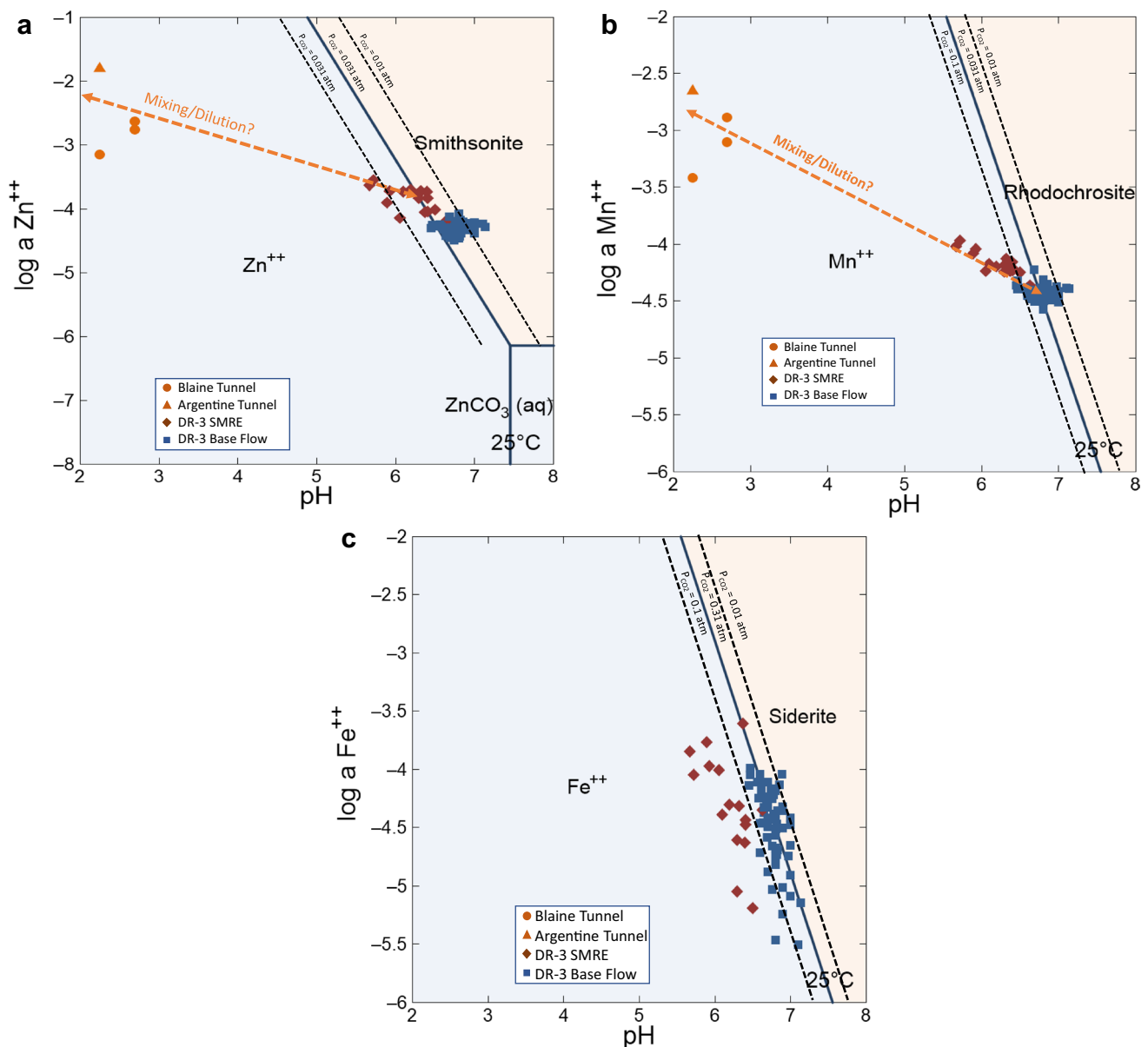
Fig. 10 Phase stability diagrams for **a** smithsonite, **b** rhodochrocite, and **c** siderite plotted with chemical data for DR-3 baseflow, DR-3 SMRE, and upper mine workings analyses plotted with respect to phase boundaries. Different assumptions of P_{CO_2} are also plotted (values within the SLT are unknown) but 0.031 atm was the average calculated for baseflow samples collected at DR-3

mostly near detections limits. The specific metal removed by adsorption depends on pH, in the general order of As being adsorbed at lower pH, then Pb, Cu, Mn, Zn, and Cd as pH increases (Langmuir 1997; Smith 1999). Other factors also influence metals removal by adsorption, but typically Mn, Ni, Zn, and Cd are only efficiently adsorbed when pH is above neutrality (Smith et al. 1992). Therefore, Cd, Mn, Ni, and Zn in the baseflow SLT mine water are mostly in the dissolved phase (Table 1, Fig. 5a–d). When waters emerge from the SLT, degassing of CO_2 and oxidation of ferrous Fe by dissolved oxygen will take place within settling ponds and result in higher pH values and precipitation of fresh iron

oxyhydroxides in the form of ferrihydrite. Research suggests that earlier settling pond design criteria for oxidation and removal of ferrous Fe (Hedin et al. 1994) may be insufficient to degas CO_2 and oxygenate CO_2-rich net-alkaline waters and use of less passive methods may be appropriate (Kirby et al. 2009). The Zn(S)/Fe(S) of suspended solids discharged directly from DR-3 during baseflow is only about 0.04 (Table 1), reflecting lower pH values where iron was precipitated and potentially increased ripening (crystallinity) as it is transported through the system. Sorption of Zn to fresh ferrihydrite will eventually occur during treatment when oxidation of ferrous Fe occurs at pH values > 7 and maximum

Table 3 Mine water concentrations from the Rico-Argentine workings and in St. Louis Tunnel discharge

Location	Sample date	Sulfate	Iron	Cadmium	Copper	Manganese	Zinc	Sum metals[c]	pH	Bicarbonate alkalinity
		mg/L	mg/L	µg/L	µg/L	µg/L	µg/L	µg/L	s.u	mg/L
Argentine Tunnel[a]	6/23/2011	6180	1950	12,000	349,000	294,000	2,460,000	2,766,000	2.25	–
Blaine Tunnel	8/4/2011	279	315	339	4140	28,200	61,700	94,379	2.25	–
Blaine Tunnel	10/3/2011	6370	1390	953	15,800	61,600	161,000	239,353	2.70	–
Blaine Tunnel	9/5/2012	–	1890	1540	26,600	107,000	226,000	361,140	2.20	< 20.0
Blaine Coffer Dam	10/6/2011	9690	2190	1180	30,300	115,000	199,000	345,480	–	–
Blaine Inflow 1[b]	8/4/2011	–	46	285	2250	17,000	51,500	71,035	3.3	–
517 Shaft	10/3/2011	1630	81.7	399	2700	23,300	67,700	94,099	–	–
517 Shaft 455 ft	10/3/2011	1650	75.3	390	2810	23,400	67,500	94,100	2.5	–
517 Shaft 475 ft	6/23/2011	618	0.445	52	55.2	4270	10,200	14,577	6.70	–
SLT Discharge (DR-3)	8/17/2011	512	1.5	19.4	4.4	2920	4630	7574	7.39	–
SLT Discharge (DR-3)	10/20/2011	535	1.09	17.5	< 5.00	2250	3810	6078	7.40	–
SLT Discharge (DR-3)	9/5/2012	622	0.349	19.5	2.5	1970	3890	5882	6.92	97.4

Data are for dissolved (0.45 µm) filtered samples

[a] Argentine Tunnel location described as "Lower Acid Pool" and not representative of flowing water

[b] Sample from water flowing into the Blaine Tunnel from a raise; other Blaine Tunnel samples from pooled water in-by of the Blaine Tunnel cofferdam

[c] Sum metals: concentrations of cadmium + copper + manganese + zinc

particulate Zn/Fe values are achieved. Dissolved Zn/Fe in the average SLT baseflow discharge is 1.4 (Table 1), and it is unlikely that Zn treatment goals will be achieved using oxidation/precipitation and settling with ferrihydrite alone.
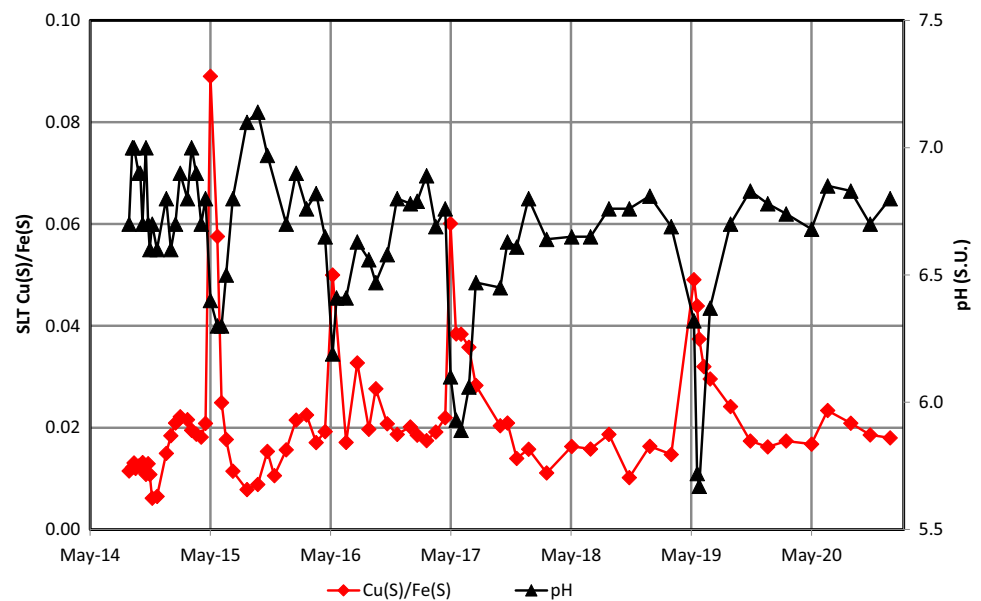
Chemistry of SLT Mine Water During SLT Snowmelt Runoff Event

Capture of snowmelt runoff in the SLT system greatly affects the chemistry of the SLT discharge water. Migration of runoff water through the upper workings during the SLT SMRE mobilizes (flushes) acid sulfate weathering products produced during the year and stored in disconnected pools and as acid precipitates on mine walls and above water levels (Desbarats and Dirom 2006; Jambor et al. 2000; Nordstrom 2011a, b). Table 3 contains the available chemical data for the upper mine workings and illustrates low pH values (2–3) and high metals concentrations. Annual flushing of the upper workings does not occur every year (Fig. 5a–d). In 2016 and 2020, the snowpack (Fig. S1) and subsequent snowmelt runoff was low and muted Zn concentration peaks occurred. In 2018, there was even less snowmelt runoff and no SLT SMRE signature was apparent in Zn concentrations (Fig. 5a). It is interesting that the year following the lack of flushing in 2018, the 2019 SLT SMRE shows even greater peak metals concentrations (Zn, Mn, Cd) suggesting the previous

year's stored acidic materials contributed to the following year's metals concentrations. The SMRE signatures for Zn and Cd (Fig. 5a, c) appear different than those of Mn, Ni, and Cu (Figs. 5b, d, 6b, respectively). Plots for Zn and Cd concentrations show abrupt rises and falls of the SLT SMRE, whereas Mn, Ni, and Cu concentrations rise abruptly, and then trail off as the SMRE wanes. The ability to see this trailing contribution is likely due to the greater dissolved 2019 SMRE peak/average baseflow concentration ratios during 2019 (6 and 8 times) for Zn and Cd (Table 1), vs. lesser 2019 SMRE peak/average baseflow concentration ratios (3 times) for Mn and Ni. The abrupt rise in these metal concentrations and low pH values represent a challenge for passive biotreatment systems that take time to acclimate to changing conditions (Dean et al. 2022; Sobolewski et al. 2022). The SLT SMRE concentrations of Zn, Mn, Cd, and Ni are almost completely in the dissolved form, as pH values are well below 7 and sorption to precipitated Fe oxides is limited.

The SLT SMRE results in a mixture of circumneutral groundwaters in equilibrium with metal carbonate minerals and snowmelt runoff that has flushed stored acidic materials from the upper mine workings formed during the fall and winter low flow seasons (acid mine drainage). These SMRE waters plot on stability diagrams for Zn and Mn (Fig. 10a, b, respectively) between the equilibrated baseflow samples (gray points) and samples collected from pools from the upper workings that contain stored acidic

Fig. 11 Time series plots of Cu(S)/Fe(S) and pH at mine drainage monitoring location DR-3. Suspended concentrations of Cu and Fe(S) were calculated as Cu(T)–Cu(D) and Fe(T)–Fe(D), respectively. Illustrates that the Cu(S)/Fe(S) ratio is highest during the SMRE, when Cu(D) is highest, and lowest pH

sulfate weathering products (gold points). Mixing of these waters controls the Zn and Mn concentrations of SMRE waters discharging from the SLT tunnel during the spring. Concentrations of Cd closely correlate with Zn during the SLT SMRE flow and baseflow. This may be due to Cd substitution in the oxidizing sphalerite (Bao et al 2021), or because Cd and Zn carbonates can form solid solutions in carbonates (Ridgley 2018) in natural fractures and the saturated zone of mine workings. Although Fe, Cu, Pb, and As are primarily contained in the suspended fractions, mixing of baseflow and SMRE waters did cause some increased dissolved concentrations of Fe, Cu, Pb, and As in 2015, 2016, 2017, and 2019 (Fig. 6a–d). Dissolved Cu concentrations increased during SMRE with peak concentrations during 2019 of 100 times the average baseflow concentration (Table 1). Spikes in total Fe concentrations outside the SLT SMRE were often related to SLT construction projects on the site and were coincident with high TSS values. These elevated total Fe concentrations co-vary with concentrations of Cu, As, and Pb (Tables S1 and S2). Copper is the metal most likely displaying sorption control on Fe-oxides at the pH values of the SMRE mine water. Suspended Cu divided by suspended Fe concentrations are plotted as a time-series in Fig. 11 to illustrate increased copper sorption during the peak SMRE periods, due to higher dissolved Cu concentrations, despite mildly acidic pH values.
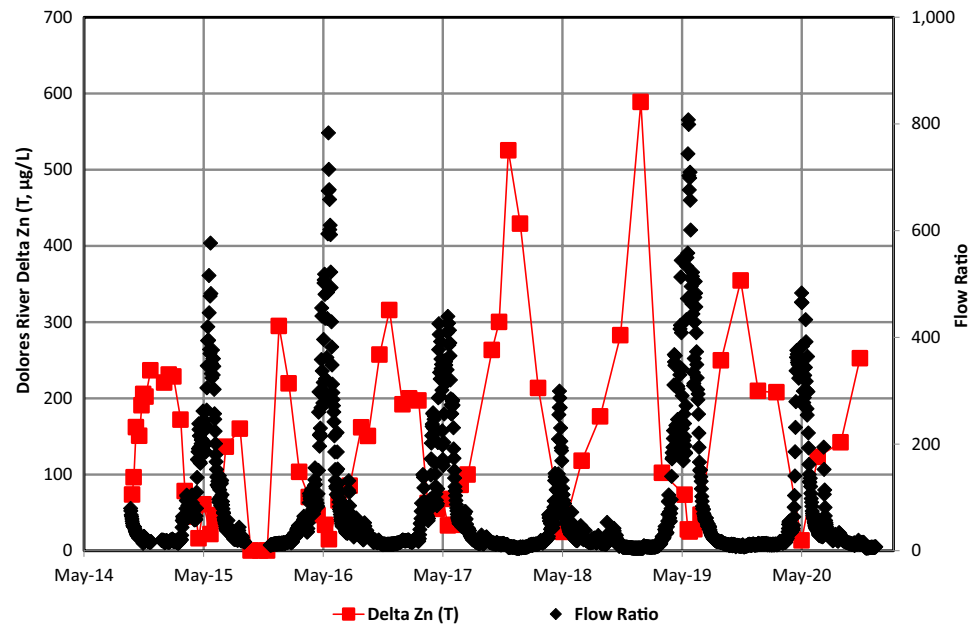
Loadings of metals to potential passive treatment systems are important for system design and are shown with time-series plots for each metal in supplemental Figs. S-2a–d and S-3a–d. Although it was originally thought that peak SLT metals concentrations occurred at the peak of the SLT hydrograph, it was determined that the peak concentrations occur on the rising limb of the SLT hydrograph (SMRE) and not the peak. Since the SLT SMRE occurs during high SLT metals concentrations and elevated SLT flows, the relative increase in load is greater than that explained by concentrations alone. Metals loading values plotted with time show more skew later in the season, as the metal concentrations decline more quickly than the falling SLT hydrograph.

Challenges in Seasonal Chemistry and Flow

Effective treatment and discharge of SLT mine water may continue to be challenging during two seasons: (1) SMRE that occurs for both the SLT and Dolores River, and (2) Dolores River low flow (late fall and winter). The SMRE for the SLT is characterized by higher mine water flows, lower pH, higher P_{CO2}, and higher metals concentrations in SLT discharge. Abrupt short-term changes in SLT chemistry during the SMRE may result in a lower treatment efficiency event while biological organisms adapt to changes in influent chemistry (Dean et al. 2022; Sobolewski et al. 2022). More frequent water management may be required during this short season. The SMRE season also correlates well with the high flow stage of the Dolores River (Fig. 8). Both the timing and intensity of the SLT SMRE and Dolores River freshet (SMRE) correlate well year-to-year during the study period. This relationship should continue indefinitely, as both SLT SMRE chemistry and peak river flows are caused by snow-melt runoff. The flow ratio of the Dolores River/SLT flow can be used to calculate the hypothetical effects of untreated SLT mine water (zero treatment efficiency) allowed to flow to the Dolores River (Fig. 12). Delta Zn is the calculated increase in Zn concentrations of mixed waters above that

Fig. 12 Time series plot of flow ratio (Dolores River flow/SLT flow) and calculated increased concentration of total Zn in mixed waters (increased above the Dolores River Zn concentration alone) if the two waters were hypothetically mixed (Delta Zn)

already existing in the upstream Dolores River water. Figure 12 shows that peak SLT metals concentrations and flow may occur during the SMRE but are offset by concurrent peak Dolores River flows and minimal delta Zn values. The SMRE season challenges the efficiency of the biotreatment cells, but there is less potential to adversely affect Dolores River water quality during this high flow period.

Low flow periods of the Dolores River occur during late fall/winter and pose the second seasonal challenge to passive biotreatment of mine water at the Rico site. Flow ratio of the Dolores River/SLT flow ranges from a low of < 10 during winter to a maximum of > 800 during the high river stage (SMRE). Fortunately, the period during low river stage also corresponds with SLT discharge with less flow, higher pH, and lower metals concentrations, where passive biotreatment of mine waters is most effective. Geothermal effects on mine water discharge will also result in relatively constant warm water influent temperatures during this cold ambient temperature period.

The consistency between the rising limb of the Dolores River hydrograph (SMRE) and the SLT SMRE low-pH high-metal concentrations response provides an opportunity to predict the timing of the abrupt SLT SMRE chemistry effects, manage mine water sampling and system operations, design future treatment systems, and develop discharge standards. Access to the site, especially the higher elevations where upper workings are located, is very difficult during winter and snowmelt conditions. Dolores River flow measured at the USGS station can be used as an indicator of the onset of SMRE conditions in the SLT mine drainage discharge. The SMRE onset is easier to detect in the Dolores

River hydrograph, as the range of flow increases 317 times for the Dolores River event, as opposed to 3.3 times for the SLT flow (2014–2020 data).

Conclusions

The SLT baseflow hydrograph is dominated by snowmelt and rainfall infiltration, groundwater recharge, and collection via the SLT system of mine workings, crosscuts, and tunnels. Another significant event occurs when snowmelt runoff predictably enters the system via preferential pathways along the Blackhawk Fault (also the alignment of the NW and SE crosscuts) and flushes acidic drainage from the upper-mine workings.

The baseflow of the SLT mine drainage is circumneutral and thermodynamic analysis suggests equilibrium with metal carbonate minerals (smithsonite, rhodochrosite, and siderite). These carbonates form as acid mine drainage is neutralized and are found naturally in the mineralized ore deposits. Other metals (Cu, Pb, and As) that occur predominantly in the suspended phase as metals are adsorbed or coprecipitated with Fe oxides.

The SMRE results in mine water discharge with lower pH and higher metals and CO_2 concentrations. This mine water results from mixing of circumneutral groundwater captured from the flooded lower mine workings with acidic salts stored in the upper mine workings and mobilized during snowmelt runoff drainage through the upper-mine workings. The SMRE is brief, predictable, and highly correlated with the Dolores River flow hydrograph.

Geothermal activity associated with this mineralized area results in near-constant year-round temperatures of SLT discharge, despite a large range in ambient air monthly average temperatures at the site.

Since snowmelt runoff rates drive the rising limb and peaks of the Dolores River hydrograph and the SLT SMRE events, Dolores River flows can be used to predict the onset and duration of the SMRE, manage sampling and operations of treatment systems, and develop seasonal discharge criteria to the Dolores River.

The challenging seasons for passive treatment systems will be: (1) the abrupt seasonal SMRE effects of SLT discharge chemistry and flow on biological treatment systems, and (2) the low flow ratio of Dolores River/SLT flow that occurs in late fall and early winter months.

References

APHA (2005) Standard Methods for the Examination of Water and Wastewater, 21st edn. American Public Health Association, Washington, DC

Bao Z, Al T, Bain J, Shrimpton HK, Finfrock YZ, Ptacek CJ, Blowes DW (2021) Sphalerite weathering controls on Zn and Cd migration in mine waste rock: an integrated study from the molecular scale to field scale. Geochem Cosmochim Acta 318(2022):1–18

Bethke CM, Farrell B (2022) The geochemist's workbench: GWB reference manual (version 16). Aqueous Solutions, LLC, Champaign

Bryant AC, Painter TH, Deems JS, Bender SM (2013) Impact of dust radiative forcing in snow on accuracy of operational runoff prediction in the Upper Colorado River Basin. Geophys Res Lett 40:3945–3949. https://doi.org/10.1002/grl.50773

Cowie R, Williams MW, Wireman M, Runkel RL (2014) Use of natural and applied tracers to guide targeted remediation efforts in an acid mine drainage system, Colorado Rockies, USA. Water 6:745–777

Cravotta CA III (2007) Passive aerobic treatment of net-alkaline iron-laden drainage from a flooded underground anthracite mine in Pennsylvania, USA. Mine Water Environ 26(3):128–149

Dean DM, Fricke JR, Riese AC, Moore TJ, Brown AR (2022) Passive treatment of circumneutral mine drainage from the St Louis Mine

Tunnel, Rico CO: Part 2—vertical biotreatment train pilot study, companion paper in this issue

Demchak J, Skousen J, McDonald LM (2004) Longevity of acid discharges from underground mines located above the regional water table. J Environ Qual 33:656–668

Desbarats AJ, Dirom GC (2006) Temporal variations in the chemistry of circum-neutral drainage from the 10-Level portal, Myra Mine, Vancouver Island, British Columbia. Appl Geochem 22:414–435

Donovan J, Leavitt B, Werner E, Perry E, McCoy K (2000) Long-term hydrogeologic and geochemical response to flooding of an abandoned below-drainage Pittsburgh coal mine. In: Proceedings of the 21st West Virginia (WV) surface mine drainage task force symposium

Hedin RS, Nairn RW, Kleinmann RLP (1994) Passive treatment of coal mine drainage. USBM IC 9389, Pittsburgh, PA

Hudson TL, Borden JC, Russ M, Bergstrom PD (1997) Controls on As, Pb, and Mn distribution in community soils of an historical mining district, southwestern Colorado. Environ Geol 33(1):25–42

Jambor JL, Nordstrom DK, Alpers CN (2000) Metal-sulfate salts from sulfide mineral oxidation. In: Alpers CN, Jambor JL, Nordstrom (eds) Sulfate minerals: crystallography, geochemistry, and environmental significance. Rev Mineral Geochem 40:303–350

Kirby CS, Dennis A, Kahler A (2009) Aeration to degas CO_2, increase pH, and increase iron oxidation rates for efficient treatment of net alkaline mine drainage. Appl Geochem 24:1175–1184

Lambert DC, Dzombak DA (2000) Evaluation of natural amelioration of acidic deep mine discharges in the Uniontown syncline, Pennsylvania. In: Proceedings of 21st WV surface mine drainage task force symposium

Langmuir D (1997) Aqueous environmental geochemistry. Prentice Hall, Englewood Cliffs

Larson PB (1987) Stable isotope and fluid inclusion investigations of epithermal vein and porphyry molybdenum mineralization in the Rico Mining District, Colorado. Econ Geol 82(8):2141–2157

Lindsay MBJ, Moncur MC, Bain JG, Jambor JL, Ptacek CJ, Blowes BW (2015) Geochemical and mineralogical aspects of sulfide mine tailings. Appl Geochem 57:157–177

McKnight ET (1974) Geology and ore deposits of the Rico District, Colorado, Geological Survey Professional Paper 723, Washington, U.S. Government Printing Office

Nairn RL (2013) Carbon dioxide impacts both passive treatment system effectiveness and carbon footprint. In: Wolkersdorfer C, Brown A, Figueroa L (eds) Proceedings of the reliable mine water technology, IMWA. https://imwa.info/docs/imwa_2013/IMWA2013_Nairn_499.pdf. Accessed 3 Aug 2021

Nordstrom DK (2011a) Mine waters: acidic to circumneutral. Elements 7:393–398

Nordstrom DK (2011b) Hydrogeochemical processes governing the origin, transport and fate of major and trace elements from mine wastes and mineralized rock to surface waters. Appl Geochem 26:1777–1791

Painter TH, Barrett AP, Landry CC, Neff JC, Cassidy MP, Lawrence CR, McBride KE, Farmer L (2007) Impact of disturbed desert soil on duration of mountain snow cover. Geophys Res Lett 34:L12502. https://doi.org/10.1029/200/2007GL30284

Painter TH, Skiles SM, Deems JS, Brandt WT, Dozier J (2018) Variations in rising limb of Colorado River snowmelt runoff hydrograph controlled by radiative forcing in snow. Geophys Res Lett 45:797–808. https://doi.org/10.1002/2017GL075826

Paser KS (1996) Characterization of and Treatment Recommendations for the St. Louis Adit Drainage and Associated Settling Ponds in Rico, Colorado. MS thesis, University of Colorado, Boulder, CO

Plumlee GS, Smith KS, Montour MR, Ficklin WH, Mosier EL (1999) Geologic controls on the composition of natural waters and mine waters draining diverse mineral-deposit types. In: Plumlee GS, Logsdon MJ (eds), The environmental geochemistry of mineral

deposits, part A, society of economic geologists, Rev Econ Geol 6A. https://doi.org/10.5382/Rev.06.19

Pratt WP, McKnight ET, DeHon RA (1969) Geologic map of the Rico Quadrangle, Dolores and Montezuma Counties, Colorado; GQ-797; U.S. Geological Survey

Ridgley V (2018) Smithsonite the calamine carbonate. Mineralexpert. org/article/smithsonite-zinc-carbonate-calamine, https://miner alexpert.org/articles (updated 22.04.2021) Accessed 16 June 2022.

Sares MA, Berkman FE, Watterson NA (2009) Statewide geothermal resource mapping in Colorado. Geotherm Resour Counc Trans 33:979–983

Smith KS, Ficklin WH, Plumlee GS, Meier AL (1992) Metal and arsenic partitioning between water and suspended sediment at mine-drainage sites in diverse geologic settings. In: Kharaka YK, Maest AS (eds) Water–rock interaction, Proceedings of the 7th international symposium on water–rock interaction, vol 1. A.A. Balkema, Rotterdam, pp 443–447

Smith KS (1999) Metal sorption on mineral surfaces: an overview with examples relating to mineral deposits. In: Plumlee GS, Logsdon MJ (eds) The environmental geochemistry of mineral deposits, part A, Rev Econ Geol, Vol 6A, pp 161–182

Sobolewski A, Riese AC, Moore TJ, Brown AR (2022) Passive treatment of circumneutral mine drainage from the St Louis Mine Tunnel, Rico CO: Part 3- horizontal wetlands treatment train pilot study, companion article in this issue

USDA Natural Resources Conservation Service (NRCS) (2021) SNOwpack TELemetry Network (SNOTEL). NRCS. https:// data.nal.usda.gov/dataset/snowpack-telemetry-network-snotel. Accessed 6 Feb 2021

USEPA (1993) Methods for Determination of Inorganic Substances in Environmental Samples, EPA/600/R-93/100 August 1993

USEPA (1994) Method 200.8: determination of trace elements in waters and wastes by inductively coupled plasma-mass spectrometry, Revision 5.4. Cincinnati, OH

USEPA (2011a) Unilateral Administrative Order for Removal Action (UAO), U.S. EPA Region 8, CERCLA Docket No. CERCLA-08 20011-0005, March 23, 2011a

USEPA (2011b) Removal Action Work Plan, Rico-Argentine Mine Site—Rico Tunnels Operable Unit OU01, Rico, Colorado, March 9, 2011b

USEPA (2012) 2011 Source Water Investigation Report, Rico-Argentine St. Louis Tunnel, Rico, Dolores County, Colorado, March 20, 2012

USEPA (2017) National Functional Guidelines for Inorganic Superfund Methods Data Review, USEPA 540-R-2017-001, January 2017

USEPA (2021a) Administrative Settlement Agreement and Order on Consent for Removal Action, U.S. EPA Region 8, CERCLA Docket No. CERCLA-08-2022-0002, Decr 6, 2021a

USEPA (2021b) Rico-Argentine Site Removal Action Work Plan, September 2021b

USGS (2022) National Water Information System data available on the World Wide Web (USGS Water Data for the Nation). http://water data.usgs.gov/nwis/. Accessed 8 Jan 2021.

Whyte J (1982) Water quantity and quality, St Louis Tunnel: Rico. Unpublished Anaconda internal memo with attachments from Jack Whyte to John Wilson dated May 21,1982.